energy&fuels

Article

pubs.acs.org/EF

Laser-Based Mass Spectrometric Determination of Aggregation Numbers for Petroleum- and Coal-Derived Asphaltenes

Qinghao Wu,[†] Andrew E. Pomerantz,[‡] Oliver C. Mullins,[‡] and Richard N. Zare*[,†]

[†]Department of Chemistry, Stanford University, Stanford, California 94305-5080, United States

[‡]Schlumberger-Doll Research Center, 1 Hampshire Street, Cambridge, Massachusetts 02139, United States

Supporting Information

ABSTRACT: Petroleum- and coal-derived asphaltenes have been studied with three laser-based mass spectrometric techniques: laser desorption ionization−mass spectrometry (LDI−MS), in which a single laser desorbs and ionizes solid analytes; surface-assisted laser desorption ionization−mass spectrometry (SALDI−MS), in which a single laser desorbs and ionizes solid analytes from an activated surface; and laser desorption laser ionization mass spectrometry (L^2MS), in which desorption and ionization are separated spatially and temporally with independent pulsed laser sources. We find that asphaltene nanoaggregates can be detected in LDI−MS and SALDI−MS under mild conditions of relatively low laser power, whereas L^2MS avoids aggregation and fragmentation, detecting asphaltenes as monomeric molecules. A comparison of the L^2MS and SALDI−MS results yields an estimate of the distribution of aggregation numbers (number of molecules comprising the nanoaggregate). The most probable aggregation number observed for nanoaggregates of petroleum asphaltenes is approximately 6−8 molecules, consistent with the Yen−Mullins model of asphaltenes and predictions from the island geometry for asphaltene molecules. Additionally, the nanoaggregates are found to be relatively monodisperse, because most aggregates observed have aggregation numbers within one molecule of the most probable. In contrast, the nanoaggregates of coal asphaltenes are found to be smaller and more polydisperse, with aggregation numbers ranging from 3 to 6 molecules. Under higher powers, SALDI−MS measurements show that nanoaggregates decompose to form small multimers and monomers, suggesting that the aggregates are bound noncovalently. Coal asphaltene nanoaggregates decompose at lower laser powers than petroleum asphaltene nanoaggregates, indicating that the coal asphaltene nanoaggregates are bound less strongly than petroleum asphaltene nanoaggregates.

INTRODUCTION

Asphaltenes continue to attract much academic and industrial interests. In the upstream oil industry, an important application of asphaltene science is the prediction of gradients in the asphaltene content of petroleum on the reservoir scale. For example, a first-principles equation of state capable of predicting these gradients is being used to assess issues, such as reservoir connectivity.[1−4] The effect of gravity is often the dominating force driving these asphaltene gradients, and the magnitudes of the gradients can be predicted only with an understanding of the size and density of asphaltene particles in crude oil. According to the Yen−Mullins model, asphaltenes exist in crude oil as three distinct particles, molecules, nanoaggregates, and clusters, with tightly constrained sizes.[5,6]

The size and mass of asphaltene molecules have been the subject of much previous work. While estimates of the average asphaltene molecular weight have varied by orders of magnitude, most recent measurements have converged on an average molecular weight near 700 Da. Measurements based on diffusion experiments, such as time-resolved fluorescence depolarization,[7,8] fluorescence correlation spectroscopy,[9−11] Taylor dispersion,[12] and nuclear magnetic resonance,[13] as well as mass spectrometry experiments involving ionization techniques, such as field ionization,[14] field desorption ionization,[15] electrospray ionization,[16] atmospheric pressure chemical ionization,[17,18] laser desorption ionization,[19−24] and laser desorption laser ionization,[25,26] generally agree on this value.

Numerous techniques have also been applied to measure asphaltene nanoaggregates, including small-angle neutron scattering (SANS) and small-angle X-ray scattering (SAXS),[27−32] direct current (DC) conductivity,[33] electrospray ionization,[34] centrifugation,[35,36] Langmuir−Blodgett films,[37,38] and reservoir gradient analysis.[2] While these analyses are more consistent than previous measurements of molecular mass, estimates of the aggregation number (number of molecules per aggregate) vary by more than a factor of 2.

Laser-based mass analyses form a diverse set of methods to characterize asphaltenes and other samples. One implementation of laser-based mass spectrometry is laser desorption laser ionization mass spectrometry (L^2MS). Here, an infrared (IR) laser is used to desorb solid asphaltenes from a surface, and following a brief time delay, an ultraviolet laser is used to ionize asphaltenes in the gas phase. This technique is known to suppress aggregation almost entirely and to minimize fragmentation, particularly if single photon ionization is employed.[39] In L^2MS experiments, the IR desorption does not generate ions at the surface of the sample, unlike laser desorption ionization−mass spectrometry (LDI−MS) and surface-assisted laser desorption ionization−mass spectrometry (SALDI−MS) experiments.[26] Ionization is delayed until the asphaltenes are dispersed in the vacuum, avoiding the

Received: September 29, 2013
Revised: December 6, 2013
Published: December 17, 2013

formation of aggregates by ion-induced dipole attractions, which occur in higher pressure ionization.[25] The short wavelength ultraviolet (UV) photon ionizes nearly all polycyclic aromatic hydrocarbons (PAHs) with relatively uniform cross-section and very little fragmentation.[49] L^2MS has been used in a variety of applications, including ancient terrestrial rocks,[40] sediments and soils,[41,42] meteorites,[43−45] interplanetary dust particles,[46,47] atmospheric aerosols,[33] stardust,[34] agricultural samples,[48] polymers,[49] natural water samples,[50] and, of course, asphaltenes.[25,26,51−53] The results from all L^2MS studies of petroleum asphaltenes are consistent with each other, showing that the most probable molecular weight of asphaltene molecules is ∼700 Da.[25,26,51−53] These studies are in agreement with the mass spectral and molecular diffusion results above. Indeed, this extensive agreement is why the debate regarding asphaltene molecular weight is viewed as largely resolved by many in the field.

Another implementation of laser-based mass spectrometry is LDI−MS. Here, a single laser beam impinges on a solid asphaltene sample resting on a metal plate, resulting in both desorption and ionization. To increase desorption and ionization efficiencies on the metal plate, SALDI−MS has been developed.[54,55] In SALDI−MS, the surface of the sample plate transfers energy to the analyte to assist with desorption and ionization. Many different substrates have been developed since the first substrate, known as desorption/ionization on silicon (DIOS), was reported in 1999.[54] The substrates reported in the literature can be roughly classified into three main types: carbon based,[56−59] semiconductor based,[54,60,61] and metal based.[62−65] With good performance on small-molecular-weight compounds, SALDI−MS offers several other advantages, including easy sample preparation, high salt tolerance, and soft ionization.[62,66]

Although much recent work has focused on asphaltenes derived from petroleum, analyses of asphaltenes derived from coal can provide insight into both the properties of asphaltenes and the response of different analytical methods. The compositions of petroleum asphaltenes and coal asphaltenes have been studied using various techniques. In fluorescence depolarization measurements, coal asphaltene molecules were found to be smaller than petroleum asphaltenes.[13] This finding was confirmed by L^2MS[55] and LDI−MS.[19−21] A study using ^{13}C nuclear magnetic resonance (NMR) showed that coal asphaltenes contain a greater percentage of aromatic carbon than petroleum asphaltenes, approximately 80% compared to 50%.[67]

Here, we report the L^2MS, LDI−MS, and SALDI−MS spectra of coal and petroleum asphaltenes. As observed previously, we find that L^2MS is sensitive to the mass of asphaltene molecules. Under certain conditions, we observe high-mass LDI−MS and SALDI−MS signals, assigned to asphaltene nanoaggregates. The study of the conditions under which nanoaggregates are observed provides insight into the strength with which asphaltene nanoaggregates are bound. A comparison of the SALDI−MS and L^2MS responses provides an estimate of the distribution of aggregation numbers.

EXPERIMENTAL SECTION

Sample Preparation. Three petroleum asphaltenes, UG8 (from Kuwait), BG5 (Kuwait), and CAL (California), have been examined. These petroleum asphaltenes were extracted from crude oils by diluting the crude oil 1:40 in *n*-heptane and then waiting 24 h. Asphaltenes were extracted from the solution by filtration through a nylon membrane possessing 0.65 μm pores. The samples were washed with additional *n*-heptane until the wash solvent was colorless. Finally, the asphaltenes were washed by Soxhlet extraction in *n*-heptane for 2 days.

Coal-derived asphaltenes from Indonesia, Tanito Harum (TH), were studied.[68] The coals were liquefied and distilled, and the distillation residue was then extracted to obtain coal-derived asphaltenes. The typical liquefaction conditions were at a temperature of 450−465 °C, a pressure of 16.8 MPa (in part from added H_2), with a gas/feed slurry ratio of 0.7 N m^3 kg^{-1}, and a coal concentration in the feed slurry of 40 wt %. The distillation residue was the fraction boiling above 538 °C. The asphaltene fraction, which is toluene-soluble and *n*-hexane-insoluble, was obtained by Soxhlet extraction of the distillation residue. Some measurements were also performed on coronene, obtained from Sigma-Aldrich (St. Louis, MO) and used without further purification.

LDI−MS and SALDI−MS. LDI−MS and SALDI−MS mass spectra were obtained using a PCS4000 mass spectrometer (Bio-Rad, Fremont, CA). In LDI−MS, an aluminum substrate (Ciphergen, Fremont, CA) was used. There is a thin overcoating of aluminum oxide on the aluminum plate, but we will refer to this plate nevertheless as an aluminum plate. In SALDI−MS, non-selective normal-phase NP20 arrays (Ciphergen, Fremont, CA) were used. The surface of the array, composed of aluminum, was modified by the addition of silicon oxide groups. Mass spectra were acquired using a pulsed nitrogen laser with a wavelength of 337 nm. The laser pulse energy was scanned from 1000 to 6000 nJ in steps of 500 nJ for petroleum asphaltenes and from 1200 to 4800 nJ in steps of 400 nJ for coal asphaltenes. The mass spectra were externally calibrated using a standard mixture of low-molecular-weight peptides (Bio-Rad). Data were acquired in the positive-ion mode from m/z 0 to 20 000 Da, focused at 4000 Da.

In LDI−MS, CAL asphaltenes were dissolved in toluene to form a solution with a concentration of 2 mg/mL. When a drop of solution of 2 μL was deposited on the surface of substrate, it will extend to a round area with a diameter of approximately 6 mm. The drop was deposited 6 times after the previous drop was dried to obtain a surface concentration (of approximately 85 $\mu g/cm^2$), comparable to a concentration used in SALDI−MS. In SALDI−MS experiments, all petroleum and coal asphaltenes were dissolved in toluene to form solutions with concentrations of 2 and 0.67 mg/mL. These solutions were used to obtain surface concentrations of 32 and 96 $\mu g/cm^2$ by depositing a drop of 2 μL solution onto a spot (outer diameter of 2.3 mm) on the sample substrate. The surface concentration of 288 $\mu g/cm^2$ was obtained by depositing 2 μL solution of 2 mg/mL 3 times after the previous drop was dried.

Two-Step L^2MS. The L^2MS technique has been described in detail elsewhere.[39] This section provides a brief description of the apparatus. A small amount of asphaltenes is fixed on a sample platter and transferred into the vacuum chamber through a vacuum interlock. A pulse of IR light from a CO_2 laser (λ = 10.6 μm; Alltec GmbH, model AL 882 APS) is focused to a spot (∼50 μm in diameter) on the sample surface using a Cassegrainian microscope objective (Ealing Optics, 15×). Desorbed neutral molecules from the platter surface form a plume in the extraction region during a time of 10−50 μs. This plume is then intersected perpendicularly by the VUV output of a pulsed F_2 excimer laser (λ = 157 nm; Coherent, Inc., ExciStar XS 200, Selmsdorf, Germany), and molecules are ionized through single-photon ionization (SPI). The resulting ions are mass-analyzed in a home-built time-of-flight mass spectrometer (TOF-MS) employing a modified Wiley−McLaren geometry. A dual microchannel plate (MCP; 20 cm^2 active area; Burle Electro-Optics, Sturbridge, MA) set in a Chevron configuration coupled with a large collector anode (Galileo TOF-4000) is used as a detector. Each recorded spectrum is averaged over 50 laser shots.

RESULTS

L^2MS and SALDI−MS Measurements of Coronene. To demonstrate the response of L^2MS and SALDI−MS, Figure 1

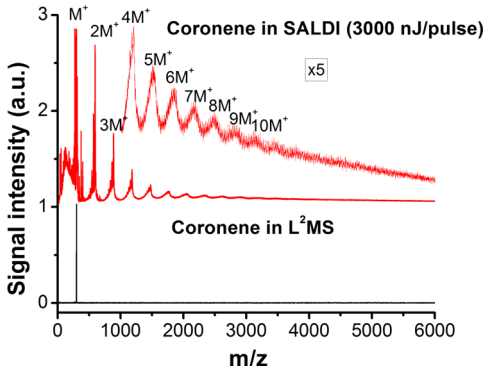

Figure 1. Coronene mass spectra from SALDI–MS (upper panel in red) and L^2MS (lower panel in black).

shows the coronene mass spectra obtained from these two analyses. In SALDI, fragments, singly charged parent ions, and aggregates with an aggregation number from 2 to 10 are all observed. This result is consistent with previously studies showing that fragmentation and aggregation are common in SALDI–MS.[21] In contrast, in L^2MS, fragmentation and aggregation are nearly completely suppressed such that only the singly charged parent ions are observed, again consistent with previous results.[21] In comparison to SALDI–MS, L^2MS is believed to suppress fragmentation because the IR-induced rapid heating favors desorption over decomposition and because the photon energy of the ionization laser is only slightly above the ionization potential of most components of asphaltenes, which results in suppression of fragmentation in the mass spectra. L^2MS is believed to minimize aggregation because the intense desorption pulse energy breaks up aggregates on the sample surface, while the delayed ionization reduces the ion-induced dipole attraction that binds together aggregates.[25]

L^2MS Measurements of Coal and Petroleum Asphaltenes. Three petroleum asphaltene samples (UG8, BG5, and CAL) and one coal asphaltene sample were scanned in L^2MS (Figure 2). Because L^2MS has a comparable sensitivity to most

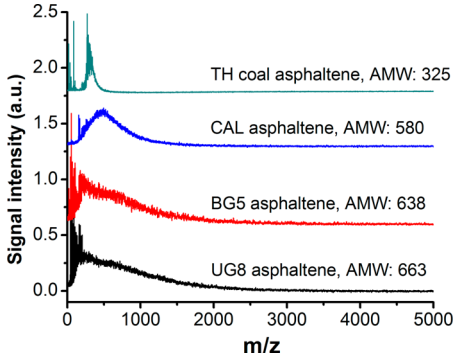

Figure 2. Mass spectra from L^2MS for four asphaltenes.

compounds in asphaltenes and can detect most of them as singly charged parent ions,[69] the mass spectra show the molecular weight distribution in these samples. To evaluate the mass distribution quantitatively, the average molecular weight (AMW) was calculated from

$$\mathrm{AMW} = \frac{\sum_i S_i (m/z)_i}{\sum_i S_i}$$

where S_i is the signal intensity and $(m/z)_i$ represents the calibrated mass-to-charge ratio in the each point i in the mass spectrum. The sum begins at mass m/z 150 (signals below this mass are believed to be fragments) and ends at m/z 2500. Calculated AMW values for TH coal asphaltenes and CAL, BG5, and UG8 asphaltenes are 325 (±16), 580 (±34), 638 (±66), and 663 (±52) Da, respectively. Generally, petroleum asphaltenes have AMW approximately double that of coal asphaltenes, which is consistent with previous studies.[8,26] The somewhat lower mass of the CAL asphaltenes relative to the other petroleum asphaltenes is consistent with its high sulfoxide content.[8]

Comparison of NP20 Arrays and Aluminum Substrates. In comparison to the aluminum substrate, the signals of NP20 arrays with no loading are more intense than those from aluminum substrates, indicating the desorption of silicon oxide groups on the aluminum surface under high laser pulse energy (see Figure S1 of the Supporting Information). However, when the NP20 arrays are loaded with asphaltenes, the background signal from silicon oxide groups is reduced (see Figure S2 of the Supporting Information). We believe that the laser pulse energy in this experiment is not high enough to desorb the silicon oxide groups when a thick layer of asphaltenes is deposited on it.

SALDI–MS Measurements of Asphaltenes from NP20 Arrays. Figure 3 shows mass spectra of CAL asphaltenes

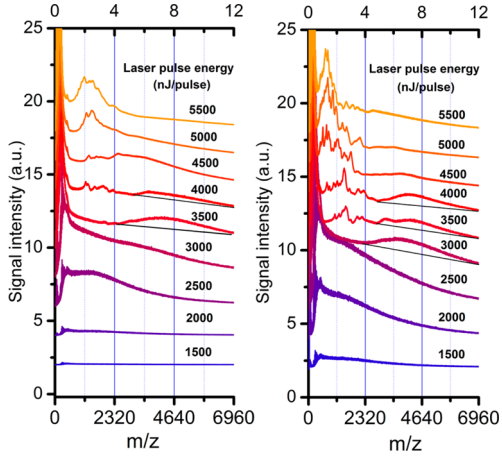

Figure 3. SALDI mass spectra for CAL asphaltenes using the Ciphergen NP20 substrate (left) and LDI mass spectra using an aluminum substrate (right) for different pulse intensities. The surface concentrations for Ciphergen NP20 substrates and aluminum substrates are 96 and 85 $\mu g/cm^2$, respectively. The top axis is the aggregation number calculated in each sample by dividing the m/z value by the AMW value. The extension of the exponential tail at aggregation numbers above 4 is shown in black in some spectra.

deposited on NP20 and aluminum substrates. NP20 is an activated surface composed of silicon oxide groups, which can assist in the desorption/ionization process; hence, measurements performed on this surface are referred to as SALDI–MS. Aluminum is an inert surface that does not assist in the desorption/ionization process; hence, measurements performed on this surface are referred to as LDI–MS. While these two methods produce different signals in the small multimer region (aggregation number < 4), both techniques observe asphaltene nanoaggregates of similar mass and at similar laser pulse energies. In addition, the overall signal

dx.doi.org/10.1021/ef401958n | Energy Fuels 2014, 28, 475–482

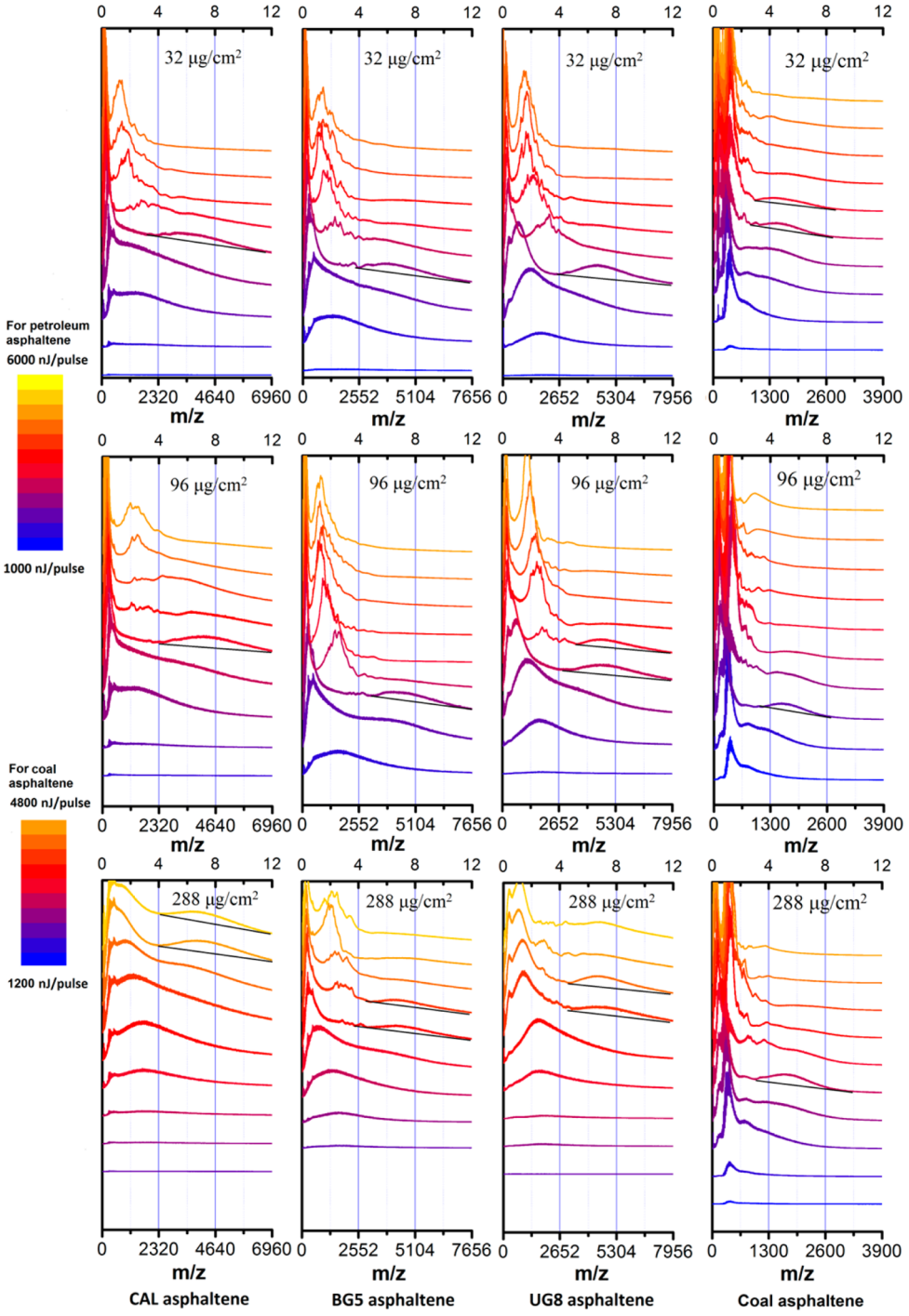

Figure 4. Mass spectra of petroleum asphaltenes (CAL, BG5, and UG8), and TH coal asphaltenes in SALDI–MS. In petroleum asphaltenes, the laser energy from blue to yellow represents the laser pulse energy from 1000 to 6000 nJ/pulse with steps of 500 nJ, whereas in coal asphaltenes, it represents the laser pulse energy from 1200 to 4800 nJ/pulse with steps of 400 nJ. The top axis is the aggregation number calculated in each sample by dividing the m/z value by the AMW value. The extension of the exponential tail at aggregation numbers above 4 is shown in black in some spectra.

strengths are similar. These consistent results suggest that the nanoaggregate signal can be confidently observed on top of the exponential tail and that the silicon oxide groups on the NP20 surface have little influence on the nanoaggregates.

Figure 4 presents the SALDI–MS spectra for the three petroleum asphaltenes, which are all similar, and for the coal asphaltenes. Most mass spectra in Figure 4 present exponential decreasing signals at an aggregation number above 3, similar to the coronene mass spectra in SALDI–MS (Figure 1). Under some conditions, such as the CAL asphaltenes at a surface concentration of 32 μg/cm^2 and laser pulse energy of 3000 nJ/pulse, a broad peak above the exponential tail is observed. We assign this signal to asphaltene nanoaggregates in the Yen–Mullins classification of asphaltenes.[5,6] With higher laser pulse energy, the intensity of the nanoaggregate peak decreases and a series of peaks from m/z 700 to 2000 appear, indicating the decomposition of the nanoaggregates. At a surface concentration of 96 μg/cm^2, the nanoaggregates appear at a laser pulse

dx.doi.org/10.1021/ef401958n | *Energy Fuels* 2014, 28, 475–482

energy of 3500 nJ/pulse and decrease above 4000 nJ/pulse. With a higher surface concentration of 288 $\mu g/cm^2$, the nanoaggregates occur at a laser pulse energy above 5000 nJ/pulse. Generally, at a higher surface concentration, the threshold laser pulse energy required to observe the nanoaggregates is higher, potentially compensating for decreased surface assistance.

Coal asphaltenes have different mass spectra from petroleum asphaltenes. In the SALDI–MS mass spectra of coal asphaltenes, intense peaks appear around its AMW, which are believed to be mostly isolated molecular ions. For coal asphaltenes with a surface concentration of 32 $\mu g/cm^2$, a broad peak is observed at a laser pulse energy near 2400 nJ/pulse. We assign this peak to nanoaggregates because the aggregation number in this peak is from 4 to 6. With a laser pulse energy higher than 3800 nJ/pulse, the nanoaggregate signal decreases, indicating nanoaggregate decomposition as observed for petroleum asphaltenes. At a surface concentration of 96 and 288 $\mu g/cm^2$, the signals from nanoaggregates are also observed but the mass range varies with different laser pulse energies.

These results suggest that the mass distribution determined in SALDI–MS is heavily dependent upon the laser pulse energy. At low laser pulse energy, the molecules and small multimers are desorbed and ionized. With higher laser pulse energy, the heavy nanoaggregates are observed as well as molecules and multimers in lower mass range. With more laser pulse energy, the nanoaggregates decompose, suggesting that they are bound noncovalently.

Aggregation Number. Figure 5 shows the SALDI–MS spectra of all samples obtained under laser pulse energy and surface concentration conditions that maximize the signal from the asphaltene nanoaggregates. The exponential tail found at all laser pulse energy and surface concentration conditions has been subtracted. The aggregation number can be estimated by dividing the peaks of the nanoaggregate mass distribution by the AMW. However, because the molecular weight distribution is broad and skewed, it is difficult to judge the range of aggregation numbers by this method.

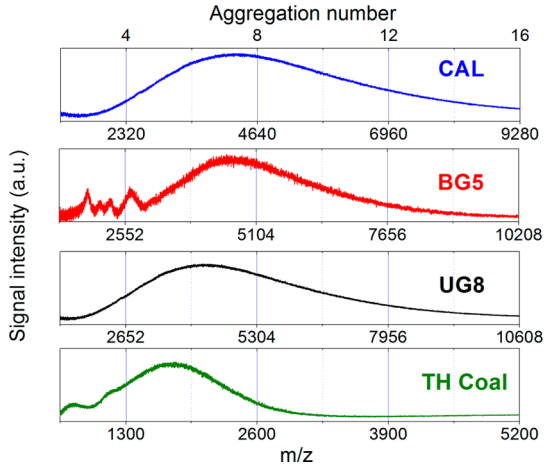

Figure 5. Aggregation number distribution for three different petroleum sources (CAL, BG5, and UG8) and one coal source (TH coal). In each case, the m/z values are divided by the value of the average molecular weight found for the sample to determine the aggregation number.

To obtain a better understanding of these nanoaggregates, a method of simulating the aggregation process was developed. The simulation is based on an assumption that every molecule has equal chance to aggregate with every other molecule in the asphaltene sample and is calculated from the L^2MS mass spectra above 150 Da. The mass distribution of dimers is simulated by combining all of the possible aggregates in the monomers, and higher aggregates are simulated by adding additional monomers.

Figure 6 shows simulated and extracted SALDI–MS spectra for all samples studied. SALDI mass spectra obtained with laser power and sample concentrations resulting in the most intense nanoaggregate peaks are shown. The simulations suggest that the aggregation number in petroleum asphaltenes is 6–8, which is within the range of aggregation numbers observed previously.[27−38] The mass distribution of nanoaggregates from petroleum asphaltenes is well-matched by the simulated distribution of a single aggregation number or a combination of two or three aggregation numbers, suggesting that petroleum

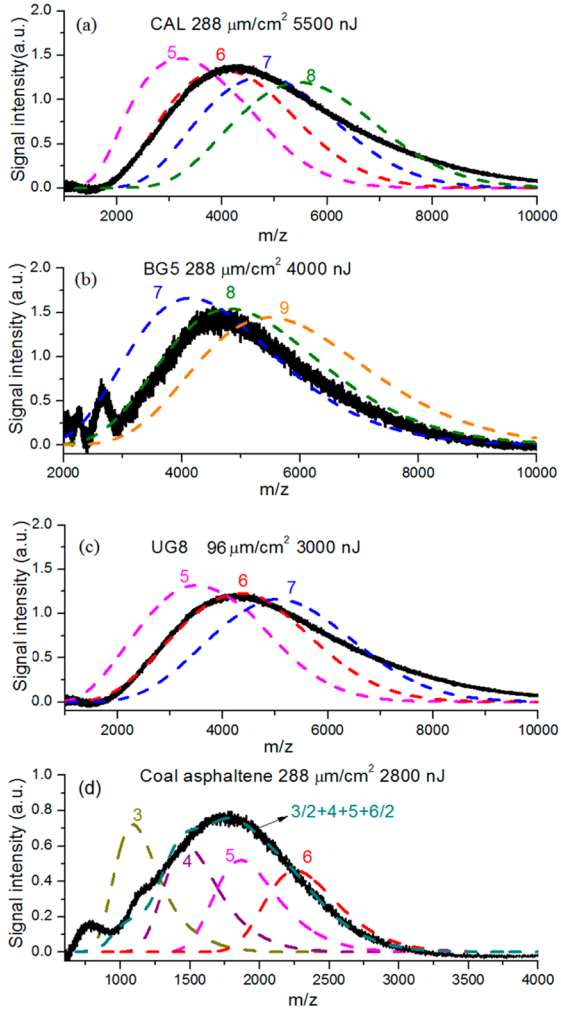

Figure 6. Comparison between simulated mass spectra to different aggregation numbers and extracted nanoaggregate signals in SALDI–MS spectra. The colored dash lines and black solid lines are simulated mass spectra and SALDI–MS spectra, respectively. The simulated mass spectra in TH coal asphaltenes are summed with half intensity of aggregation numbers of 3 and 6 and full intensity of aggregation numbers of 4 and 5 (green dashed line in panel d).

dx.doi.org/10.1021/ef401958n | Energy Fuels 2014, 28, 475–482

asphaltene nanoaggregates are relatively monodisperse. In contrast, the mass distribution of nanoaggregates from coal asphaltenes is not well-matched by the simulated distribution of a single aggregation number but is instead fit well by a sum of aggregation numbers from 3 to 6, suggesting that coal asphaltene nanoaggregates are more polydisperse.

The aggregation numbers observed here are similar to those reported with some other techniques. Results from SANS and SAXS show that the nanoaggregates have a structure of disk shape. The total radius of the disk is around 3.2 nm, and the height is around 0.67 nm. The estimated molecular weight of nanoaggregates is 16 kDa, with an aggregation number of around 20.[31] In the results obtained by direct-current electrical conductivity, the aggregation number is less than 10.[33] The NMR diffusion study[70] and equation of state approach[71] give an aggregation number of ∼8, which is very similar to our study.

DISCUSSION AND CONCLUSION

We have presented mass spectra of petroleum- and coal-derived asphaltenes obtained with three variations of laser-based mass spectrometry: LDI−MS, in which a single laser pulse desorbs and ionizes analytes deposited on an inert surface; SALDI−MS, in which a single laser pulse desorbs and ionizes analytes deposited on an activated surface; and L^2MS, in which the desorption and ionization processes are spatially and temporally separated using two independent pulsed laser sources. L^2MS detects asphaltenes as singly charged molecular ions, suppressing both fragmentation and aggregation. We found AMW values near 650 Da for UG8 and BG5 petroleum asphaltenes, whereas CAL petroleum asphaltenes are found to be slightly smaller (580 Da) and coal asphaltenes (325 Da) are found to be approximately half the size. LDI−MS and SALDI−MS measurements at low laser pulse energy revealed intense signals at higher mass. Those signals are assigned to asphaltene nanoaggregates in the Yen−Mullins model.[5,6] A comparison between the aggregate mass (SALDI−MS) and molecular mass (L^2MS) suggests that nanoaggregates of petroleum asphaltenes are relatively monodisperse and contain 6−8 molecules, while nanoaggregates of coal asphaltenes are relatively polydisperse and contain 3−6 molecules. These aggregation numbers are consistent with some previous measurements,[27−38] the Yen−Mullins model,[5,6] and with expectations for island geometries of asphaltene molecules.[72] The agreement of these disparate measurements suggests that the charged asphaltene nanoaggregates detected here are representative of the asphaltene nanoaggregates formed in crude oil. These nanoaggregates are broken apart at higher laser pulse energies, suggesting that they are held together noncovalently. Coal asphaltene nanoaggregates break apart at relatively low laser pulse energies, indicating that they are bound more weakly than petroleum asphaltene nanoaggregates. These results attest to the versatility of laser-based mass spectrometry for asphaltene analysis, because asphaltenes can be detected as either isolated molecules or nanoaggregates.

ASSOCIATED CONTENT

Supporting Information

Mass spectra for Ciphergen NP20 substrate (black) and aluminum substrate (red), each with no loading, at a laser pulse energy of 4500 nJ per pulse (337 nm) (Figure S1) and mass spectra from Ciphergen NP20 with no loading (red) and UG8 asphaltene loading (black) at a laser pulse energy of 4000 nJ/pulse (Figure 2). This material is available free of charge via the Internet at http://pubs.acs.org.

AUTHOR INFORMATION

Corresponding Author

*Telephone: 650-723-3062. E-mail: zare@stanford.edu.

Notes

The authors declare no competing financial interest.

ACKNOWLEDGMENTS

We are grateful to John Whitin, School of Medicine, Stanford University, for assistance in performing SALDI−MS measurements.

REFERENCES

(1) Zuo, J. Y.; Mullins, O. C.; Freed, D.; Elshahawi, H.; Dong, C.; Seifert, D. J. Advances in the Flory−Huggins−Zuo equation of state for asphaltene gradients and formation evaluation. *Energy Fuels* **2012**, *27* (4), 1722−1735.

(2) Mullins, O. C.; Betancourt, S. S.; Cribbs, M. E.; Dubost, F. X.; Creek, J. L.; Andrews, A. B.; Venkataramanan, L. The colloidal structure of crude oil and the structure of oil reservoirs. *Energy Fuels* **2007**, *21* (5), 2785−2794.

(3) Pomerantz, A. E.; Ventura, G. T.; McKenna, A. M.; Cañas, J. A.; Auman, J.; Koerner, K.; Curry, D.; Nelson, R. K.; Reddy, C. M.; Rodgers, R. P.; Marshall, A. G.; Peters, K. E.; Mullins, O. C. Combining biomarker and bulk compositional gradient analysis to assess reservoir connectivity. *Org. Geochem.* **2010**, *41* (8), 812−821.

(4) Andrews, A. B.; McClelland, A.; Korkeila, O.; Demidov, A.; Krummel, A.; Mullins, O. C.; Chen, Z. Molecular orientation of asphaltenes and PAH model compounds in Langmuir−Blodgett films using sum frequency generation spectroscopy. *Langmuir* **2011**, *27* (10), 6049−6058.

(5) Mullins, O. C. The modified Yen model. *Energy Fuels* **2010**, *24*, 2179−2207.

(6) Mullins, O. C.; Sabbah, H.; Eyssautier, J.; Pomerantz, A. E.; Barre, L.; Andrews, A. B.; Ruiz-Morales, Y.; Mostowfi, F.; McFarlane, R.; Goual, L.; Lepkowicz, R.; Cooper, T.; Orbulescu, J.; Leblanc, R. M.; Edwards, J.; Zare, R. N. Advances in asphaltene science and the Yen−Mullins model. *Energy Fuels* **2012**, *26* (7), 3986−4003.

(7) Groenzin, H.; Mullins, O. C. Asphaltene molecular size and structure. *J. Phys. Chem. A* **1999**, *103* (50), 11237−11245.

(8) Groenzin, H.; Mullins, O. C. Molecular size and structure of asphaltenes from various sources. *Energy Fuels* **2000**, *14* (3), 677−684.

(9) Andrews, A. B.; Guerra, R. E.; Mullins, O. C.; Sen, P. N. Diffusivity of asphaltene molecules by fluorescence correlation spectroscopy. *J. Phys. Chem. A* **2006**, *110* (26), 8093−8097.

(10) Schneider, M. H.; Andrews, A. B.; Mitra-Kirtley, S.; Mullins, O. C. Asphaltene molecular size by fluorescence correlation spectroscopy. *Energy Fuels* **2007**, *21* (5), 2875−2882.

(11) Guerra, R. E.; Ladavac, K.; Andrews, A. B.; Mullins, O. C.; Sen, P. N. Diffusivity of coal and petroleum asphaltene monomers by fluorescence correlation spectroscopy. *Fuel* **2007**, *86* (12−13), 2016−2020.

(12) Wargadalam, V. J.; Norinaga, K.; Lino, M. Size and shape of a coal asphaltene studied by viscosity and diffusion coefficient measurements. *Fuel* **2002**, *81* (11−12), 1403−1407.

(13) Lisitza, N. V.; Freed, D. E.; Sen, P. N.; Song, Y.-Q. Study of asphaltene nanoaggregation by nuclear magnetic resonance (NMR). *Energy Fuels* **2009**, *23*, 1189−1193.

(14) Boduszynski, M. M. Composition of heavy petroleums. 1. Molecular-weight, hydrogen deficiency, and heteroatom concentration as a function of atmospheric equivalent boiling point up to 1400 °F (760 °C). *Energy Fuels* **1987**, *1* (1), 2−11.

(15) Qian, K.; Edwards, K. E.; Siskin, M.; Olmstead, W. N.; Mennito, A. S.; Dechert, G. J.; Hoosain, N. E. Desorption and ionization of

heavy petroleum molecules and measurement of molecular weight distributions. *Energy Fuels* **2007**, *21* (2), 1042−1047.
(16) Mullins, O. C.; Martinez-Haya, B.; Marshall, A. G. Contrasting perspective on asphaltene molecular weight. This comment vs the overview of A. A. Herod, K. D. Bartle, and R. Kandiyoti. *Energy Fuels* **2008**, *22* (3), 1765−1773.
(17) Cunico, R. L.; Sheu, E. Y.; Mullins, O. C. Molecular weight measurement of UG8 asphaltene using APCI mass spectroscopy. *Pet. Sci. Technol.* **2004**, *22* (7−8), 787−798.
(18) Sheu, E. Y.; Mullins, O. Frequency-dependent conductivity of utah crude oil asphaltene and deposit. *Energy Fuels* **2004**, *18* (5), 1531−1534.
(19) Hortal, A. R.; Martinez-Haya, B.; Lobato, M. D.; Pedrosa, J. M.; Lago, S. On the determination of molecular weight distributions of asphaltenes and their aggregates in laser desorption ionization experiments. *J. Mass Spectrom.* **2006**, *41* (7), 960−968.
(20) Hortal, A. R.; Hurtado, P.; Martinez-Haya, B.; Mullins, O. C. Molecular-weight distributions of coal and petroleum asphaltenes from laser desorption/ionization experiments. *Energy Fuels* **2007**, *21* (5), 2863−2868.
(21) Martinez-Haya, B.; Hortal, A. R.; Hurtado, P.; Lobato, M. D.; Pedrosa, J. M. Laser desorption/ionization determination of molecular weight distributions of polyaromatic carbonaceous compounds and their aggregates. *J. Mass Spectrom.* **2007**, *42* (6), 701−713.
(22) Tanaka, R.; Sato, S.; Takanohashi, T.; Hunt, J. E.; Winans, R. E. Analysis of the molecular weight distribution of petroleum asphaltenes using laser desorption−mass spectrometry. *Energy Fuels* **2004**, *18* (5), 1405−1413.
(23) Acevedo, S.; Gutierrez, L. B.; Negrin, G.; Pereira, J. C.; Mendez, B.; Delolme, F.; Dessalces, G.; Broseta, D. Molecular weight of petroleum asphaltenes: A comparison between mass spectrometry and vapor pressure osmometry. *Energy Fuels* **2005**, *19* (4), 1548−1560.
(24) Al-Muhareb, E.; Morgan, T. J.; Herod, A. A.; Kandiyoti, R. Characterization of petroleum asphaltenes by size exclusion chromatography, UV−fluorescence and mass spectrometry. *Pet. Sci. Technol.* **2007**, *25* (1−2), 81−91.
(25) Pomerantz, A. E.; Hammond, M. R.; Morrow, A. L.; Mullins, O. C.; Zare, R. N. Two-step laser mass spectrometry of asphaltenes. *J. Am. Chem. Soc.* **2008**, *130* (23), 7216−7217.
(26) Pomerantz, A. E.; Hammond, M. R.; Morrow, A. L.; Mullins, O. C.; Zare, R. N. Asphaltene molecular-mass distribution determined by two-step laser mass spectrometry. *Energy Fuels* **2009**, *23*, 1162−1168.
(27) Fenistein, D.; Barre, L. Experimental measurement of the mass distribution of petroleum asphaltene aggregates using ultracentrifugation and small-angle X-ray scattering. *Fuel* **2001**, *80* (2), 283−287.
(28) Gawrys, K. L.; Kilpatrick, P. K. Asphaltenic aggregates are polydisperse oblate cylinders. *J. Colloid Interface Sci.* **2005**, *288* (2), 325−334.
(29) Wiehe, I. A.; Liang, K. S. Asphaltenes, resins, and other petroleum macromolecules. *Fluid Phase Equilib.* **1996**, *117* (1−2), 201−210.
(30) Sheu, E. Y. Petroleomics and characterization of asphaltene aggregates using small angle scattering. In *Asphaltene, Heavy Oils and Petroleomics*; Springer: New York, 2007.
(31) Eyssautier, J.; Levitz, P.; Espinat, D.; Jestin, J.; Gummel, J.; Grillo, I.; Barre, L. Insight into asphaltene nanoaggregate structure inferred by small angle neutron and X-ray scattering. *J. Phys. Chem. B* **2011**, *115* (21), 6827−6837.
(32) Eyssautier, J.; Frot, D.; Barre, L. Structure and dynamic properties of colloidal asphaltene aggregates. *Langmuir* **2012**, *28* (33), 11997−12004.
(33) Zeng, H.; Song, Y.-Q.; Johnson, D. L.; Mullins, O. C. Critical nanoaggregate concentration of asphaltenes by direct-current (DC) electrical conductivity. *Energy Fuels* **2009**, *23*, 1201−1208.
(34) McKenna, A. M.; Donald, L. J.; Fitzsimmons, J. E.; Juyal, P.; Spicer, V.; Standing, K. G.; Marshall, A. G.; Rodgers, R. P. Heavy petroleum composition. 3. asphaltene aggregation. *Energy Fuels* **2013**, *27* (3), 1246−1256.
(35) Indo, K.; Ratulowski, J.; Dindoruk, B.; Gao, J.; Zuo, J.; Mullins, O. C. Asphaltene nanoaggregates measured in a live crude oil by centrifugation. *Energy Fuels* **2009**, *23*, 4460−4469.
(36) Mostowfi, F.; Indo, K.; Mullins, O. C.; McFarlane, R. Asphaltene nanoaggregates studied by centrifugation. *Energy Fuels* **2009**, *23*, 1194−1200.
(37) Orbulescu, J.; Mullins, O. C.; Leblanc, R. M. Surface chemistry and spectroscopy of UG8 asphaltene langmuir film, part 1. *Langmuir* **2010**, *26* (19), 15257−15264.
(38) Orbulescu, J.; Mullins, O. C.; Leblanc, R. M. Surface chemistry and spectroscopy of UG8 asphaltene langmuir film, part 2. *Langmuir* **2010**, *26* (19), 15265−15271.
(39) Wu, Q.; Pomerantz, A.; Mullins, O.; Zare, R. Minimization of fragmentation and aggregation by laser desorption laser ionization mass spectrometry. *J. Am. Soc. Mass Spectrom.* **2013**, 1−7.
(40) Mahajan, T. B.; Plows, F. L.; Gillette, J. S.; Zare, R. N.; Logan, G. A. Comparison of microprobe two-step laser desorption/laser ionization mass spectrometry and gas chromatography/mass spectrometry studies of polycyclic aromatic hydrocarbons in ancient terrestrial rocks. *J. Am. Soc. Mass Spectrom.* **2001**, *12* (9), 989−1001.
(41) Fye, J. L.; Nelson, H. H.; Mowery, R. L.; Baronavski, A. P.; Callahan, J. H. Scanning ultraviolet two-step laser mass spectroscopy of polycyclic aromatic hydrocarbon distributions on creosote-contaminated soil particles. *Anal. Chem.* **2002**, *74* (13), 3019−3029.
(42) Gillette, J. S.; Luthy, R. G.; Clemett, S. J.; Zare, R. N. Direct observation of polycyclic aromatic hydrocarbons on geosorbents at the subparticle scale. *Environ. Sci. Technol.* **1999**, *33* (8), 1185−1192.
(43) Clemett, S. J.; Zare, R. N. Microprobe two-step laser mass spectrometry as an analytical tool for meteoritic samples. In *Molecules in Astrophysics: Probes and Processes*; Springer: New York, 1997; pp 305−320.
(44) Plows, F. L.; Elsila, J. E.; Zare, R. N.; Buseck, P. R. Evidence that polycyclic aromatic hydrocarbons in two carbonaceous chondrites predate parent-body formation. *Geochim. Cosmochim. Acta* **2003**, *67* (7), 1429−1436.
(45) Spencer, M. K.; Hammond, M. R.; Zare, R. N. Laser mass spectrometric detection of extraterrestrial aromatic molecules: Mini-review and examination of pulsed heating effects. *Proc. Natl. Acad. Sci. U. S. A.* **2008**, *105* (47), 18096−18101.
(46) Clemett, S. J.; Maechling, C. R.; Zare, R. N.; Swan, P. D.; Walker, R. M. Identification of complex aromatic molecules in individual interplanetary dust particles. *Science* **1993**, *262* (5134), 721−725.
(47) Greenberg, J. M.; Gillette, J. S.; Caro, G. M. M.; Mahajan, T. B.; Zare, R. N.; Li, A. G.; Schutte, W. A.; de Groot, M.; Mendoza-Gomez, C. Ultraviolet photoprocessing of interstellar dust mantles as a source of polycyclic aromatic hydrocarbons and other conjugated molecules. *Astrophys. J.* **2000**, *531* (1), L71−L73.
(48) Orea, J. M.; Montero, C.; Jimenez, J. B.; Urena, A. G. Analysis of *trans*-resveratrol by laser desorption coupled with resonant ionization spectrometry. Application to *trans*-resveratrol content in vine leaves and grape skin. *Anal. Chem.* **2001**, *73* (24), 5921−5929.
(49) Zhan, Q.; Zenobi, R.; Wright, S. J.; LangridgeSmith, P. R. R. Spatially resolved in-situ analysis of polymer additives by two-step laser mass spectrometry. *Macromolecules* **1996**, *29* (24), 7865−7871.
(50) Bucheli, T. D.; Haefliger, O. P.; Dietiker, R.; Zenobi, R. Analysis of water contaminants and natural water samples using two-step laser mass spectrometry. *Anal. Chem.* **2000**, *72* (15), 3671−3677.
(51) Sabbah, H.; Morrow, A. L.; Pomerantz, A. E.; Zare, R. N. Evidence for island structures as the dominant architecture of asphaltenes. *Energy Fuels* **2011**, *25* (4), 1597−1604.
(52) Sabbah, H.; Morrow, A. L.; Pomerantz, A. E.; Mullins, O. C.; Tan, X.; Gray, M. R.; Azyat, K.; Tykwinski, R. R.; Zare, R. N. Comparing laser desorption/laser ionization mass spectra of asphaltenes and model compounds. *Energy Fuels* **2010**, *24*, 3589−3594.
(53) Hurtado, P.; Gamez, F.; Martinez-Haya, B. One- and two-step ultraviolet and infrared laser desorption ionization mass spectrometry of asphaltenes. *Energy Fuels* **2010**, *24*, 6067−6073.

(54) Wei, J.; Buriak, J. M.; Siuzdak, G. Desorption−ionization mass spectrometry on porous silicon. *Nature* **1999**, *399* (6733), 243−246.
(55) Shen, Z. X.; Thomas, J. J.; Averbuj, C.; Broo, K. M.; Engelhard, M.; Crowell, J. E.; Finn, M. G.; Siuzdak, G. Porous silicon as a versatile platform for laser desorption/ionization mass spectrometry. *Anal. Chem.* **2001**, *73* (3), 612−619.
(56) Dattelbaum, A. M.; Iyer, S. Surface-assisted laser desorption/ionization mass spectrometry. *Expert Rev. Proteomics* **2006**, *3* (1), 153−161.
(57) Najam-ul-Haq, M.; Rainer, M.; Szabo, Z.; Vallant, R.; Huck, C. W.; Bonn, G. K. Role of carbon nano-materials in the analysis of biological materials by laser desorption/ionization−mass spectrometry. *J. Biochem. Biophys. Methods* **2007**, *70* (2), 319−328.
(58) Tang, H.-W.; Ng, K.-M.; Lu, W.; Che, C.-M. Ion desorption efficiency and internal energy transfer in carbon-based surface-assisted laser desorption/ionization mass spectrometry: Desorption mechanism(s) and the design of SALDI substrates. *Anal. Chem.* **2009**, *81* (12), 4720−4729.
(59) Zhang, H.; Cha, S.; Yeung, E. S. Colloidal graphite-assisted laser desorption/ionization MS and MS^n of small molecules. 2. Direct profiling and MS imaging of small metabolites from fruits. *Anal. Chem.* **2007**, *79* (17), 6575−6584.
(60) Lewis, W. G.; Shen, Z. X.; Finn, M. G.; Siuzdak, G. Desorption/ionization on silicon (DIOS) mass spectrometry: Background and applications. *Int. J. Mass Spectrom.* **2003**, *226* (1), 107−116.
(61) Northen, T. R.; Woo, H.-K.; Northen, M. T.; Nordstroem, A.; Uritboonthail, W.; Turner, K. L.; Siuzdak, G. High surface area of porous silicon drives desorption of intact molecules. *J. Am. Soc. Mass Spectrom.* **2007**, *18* (11), 1945−1949.
(62) Law, K. P.; Larkin, J. R. Recent advances in SALDI−MS techniques and their chemical and bioanalytical applications. *Anal. Bioanal. Chem.* **2011**, *399* (8), 2597−2622.
(63) Kruse, R. A.; Li, X. L.; Bohn, P. W.; Sweedler, J. V. Experimental factors controlling analyte ion generation in laser desorption/ionization mass spectrometry on porous silicon. *Anal. Chem.* **2001**, *73* (15), 3639−3645.
(64) Piret, G.; Coffinier, Y.; Roux, C.; Melnyk, O.; Boukherroub, R. Biomolecule and nanoparticle transfer on patterned and heterogeneously wetted superhydrophobic silicon nanowire surfaces. *Langmuir* **2008**, *24* (5), 1670−1672.
(65) Yan, B.; Zhu, Z.-J.; Miranda, O. R.; Chompoosor, A.; Rotello, V. M.; Vachet, R. W. Laser desorption/ionization mass spectrometry analysis of monolayer-protected gold nanoparticles. *Anal. Bioanal. Chem.* **2010**, *396* (3), 1025−1035.
(66) Lim, A. Y.; Ma, J.; Boey, Y. C. F. Development of nanomaterials for SALDI−MS analysis in forensics. *Adv. Mater.* **2012**, *24* (30), 4211−4216.
(67) Andrews, A. B.; Edwards, J. C.; Pomerantz, A. E.; Mullins, O. C.; Nordlund, D.; Norinaga, K. Comparison of coal-derived and petroleum asphaltenes by ^{13}C nuclear magnetic resonance, DEPT, and XRS. *Energy Fuels* **2011**, *25* (7), 3068−3076.
(68) Badre, S.; Goncalves, C. C.; Norinaga, K.; Gustavson, G.; Mullins, O. C. Molecular size and weight of asphaltene and asphaltene solubility fractions from coals, crude oils and bitumen. *Fuel* **2006**, *85* (1), 1−11.
(69) Sabbah, H.; Pomerantz, A. E.; Wagner, M.; Muellen, K.; Zare, R. N. Laser desorption single-photon ionization of asphaltenes: Mass range, compound sensitivity, and matrix effects. *Energy Fuels* **2012**, *26* (6), 3521−3526.
(70) Freed, D. E.; Lisitza, N. V.; Sen, P. N.; Song, Y.-Q. Asphaltene molecular composition and dynamics of oils from NMR diffusion measurements. In *Asphaltenes, Heavy Oils, and Petroleomics*; Springer: New York, 2007.
(71) Betancourt, S. S.; Ventura, G. T.; Pomerantz, A. E.; Viloria, O.; Dubost, F. X.; Zuo, J.; Monson, G.; Bustamante, D.; Purcell, J. M.; Nelson, R. K.; Rodgers, R. P.; Reddy, C. M.; Marshall, A. G.; Mullins, O. C. Nanoaggregates of asphaltenes in a reservoir crude oil and reservoir connectivity. *Energy Fuels* **2009**, *23*, 1178−1188.
(72) Andreatta, G.; Bostrom, N.; Mullins, O. C. High-Q ultrasonic determination of the critical nanoaggregate concentration of asphaltenes and the critical micelle concentration of standard surfactants. *Langmuir* **2005**, *21* (7), 2728−2736.